ELSEVIER

Global and Planetary Change 32 (2002) 361–374

GLOBAL AND PLANETARY CHANGE

www.elsevier.com/locate/gloplacha

Desert margins near the Chinese Loess Plateau during the mid-Holocene and at the Last Glacial Maximum: a model–data intercomparison

Andrew B.G. Bush [a,*], Dean Rokosh [a], Nathaniel W. Rutter [a], T. Bryant Moodie [b]

[a] *Department of Earth and Atmospheric Sciences, University of Alberta, 126 Earth Science Building, Edmonton, Alberta, Canada T6G 2E3*
[b] *Department of Mathematical Sciences, University of Alberta, Central Academic Building, Edmonton, Alberta, Canada T6G 2G1*

Accepted 16 October 2001

Abstract

Expansion and contraction of desert margins around the globe have been inferred from a variety of proxy data and have since been linked, particularly in northern China and in the sub-Sahel, to changes in freshwater flux, vegetation cover, sea surface temperatures and, perhaps most importantly, monsoon circulations. We present a direct comparison of results from numerical general circulation model experiments for the mid-Holocene and for the Last Glacial Maximum (LGM) with the climatic conditions that have been inferred from loess–paleosol sequences taken from the Chinese Loess Plateau. During the mid-Holocene in northern China, the northwestward migration of the southeast desert margin that has been suggested by grain size analysis is also expressed in the model results. There is a statistically significant wetting of the Plateau region, and increased soil moisture is a consequence of an enhanced summer monsoon whose latent heat release deepens the cyclonic Tibetan low and brings increased low-level convergence and precipitation to the area. North of the desert region, this circulation dries the soil through enhanced atmospheric subsidence, although the northern margin of the desert does not migrate significantly. Expansion of the desert margin toward the southeast at the LGM is small, but there is a statistically significant drying of the Plateau. The local hydrological cycle is reduced, and there is an increase in large-scale atmospheric subsidence over the region that is caused by the presence of the Fennoscandian ice sheet upwind. Model results therefore suggest that, in addition to local micro- and mesoclimatic conditions, regional effects, such as monsoon circulations and distal orography, are also important factors in determining the location of desert margins.

Keywords: Last Glacial Maximum and Holocene desert margin; Chinese Loess Plateau; Model–data intercomparison

1. Introduction

There are many indicators of climate change contained within the geological record. One example is the set of loess–paleosol sequences on the Loess Plateau of northern China. These sequences give a high resolution record of alternation between relatively dry, loess-forming conditions typical of glacial periods, and low-accumulation, soil-forming conditions typical of interglacial periods (e.g., Rutter, 1992; Ding et al., 1993). Information from these sequences has been used to reconstruct climatic history of the region surrounding the Loess Plateau through the last glacial cycle (e.g., Vandenberghe et al., 1997; Sun et al., 1999; Lu et al., 1999, 2000). In particular, sand

* Corresponding author.
E-mail address: andrew.bush@ualberta.ca (A.B.G. Bush).

0921-8181/02/$ - see front matter
PII: S0921-8181(02)00076-0

content of the loess deposits has been used to infer proximity to the desert margin (Ding et al., 1999). Further, the loess sequences have been correlated with other global records, such as deep sea cores (e.g., Porter and An, 1995; Guo et al., 1998; Rack et al., 2000), and may to some degree be taken as a proxy record for large-scale climate change.

However, wind strength and direction govern the grain sizes and volume fraction of suspended particles, as well as the net amount of particles deposited in a particular geographic location. For the Loess Plateau, reconstructions indicate that the climatological westerly and northwesterly winds have probably been the most important in governing deposition through the last glacial cycle (e.g., Lu and Sun, 2000). Other factors that play a role in particle deposition are continental aridity, vegetation feedbacks, and the atmosphere's loading of greenhouse gases, which plays an indirect role by regulating the global hydrological cycle as well as surface vegetation (e.g., Mahowald et al., 1999; Texier et al., 2000). It is now apparent that all of the above factors have changed continuously throughout the late Quaternary (e.g., Wright et al., 1993).

During the mid-Holocene, changes in the Earth's orbital parameters amplified the seasonal cycle and strengthened monsoon circulations, particularly in southeast Asia (e.g., Kutzbach and Otto-Bliesner, 1982; Prell and Kutzbach, 1992). The geological record indicates that the arid regions east of the Helan Mountains were at that time covered by grass (e.g., Ding et al., 1999), and this suggests a much greater freshwater flux over the area (if desertification is not attributed to human activity). It is likely, therefore, that the mid-Holocene climate exhibited changes in monsoon winds as well as changes in freshwater flux and soil moisture.

At the Last Glacial Maximum (LGM), both continental aridity and strong atmospheric winds have been inferred from a variety of proxy data (e.g., Molina-Cruz, 1977; Petit et al., 1981, 1990; Sarnthein et al., 1981; Pedersen, 1983). Atmospheric winds have been simulated in numerical models configured for the LGM, and Northern Hemisphere ice sheets and surface conditions are known to have played a major role in redirecting them (e.g., Kutzbach and Wright, 1985; Manabe and Broccoli, 1985; Hall et al., 1996; Broccoli and Manabe, 1997; Bush and Philander, 1999; Wyrwoll et al., 2000). Wind changes would alter the hydrological balance over the Loess Plateau, and it has been suggested from field data that the desert margin at the LGM was either close to its present location or further to the southeast (depending on where the modern margin is placed; Zhao, 1986; Sun and Ding, 1998; Sun et al., 1998a; Ding et al., 1999).

In this study, we compare the field results that indicate northwest to southeast migration of the desert margin with the results of numerical simulations performed with a coupled atmosphere–ocean general circulation model (GCM). Given the equivalent spatial resolution of GCMs, we are not, in this study, able to specify exactly where a desert margin is, nor are we invoking any arguments for changes on the meso- to microscale. As will be shown, however, the simulated changes in area-averaged soil moisture are in agreement with the field data, are statistically significant and, to first order, are linked to changes in large-scale atmospheric circulation patterns.

The outline of the paper is as follows. Section 2 briefly describes the numerical model used. Section 3 summarizes the results from the field work and grain size analysis. Sections 4 and 5 describe the model results for the mid-Holocene and LGM simulations, respectively. A discussion follows in Section 6, and conclusions are presented in Section 7.

2. Model description

The numerical model is a global, fully coupled, atmosphere–ocean GCM. It has been configured for three different time slices: the LGM (21,000 years B.P.), the mid-Holocene (6000 years B.P.), and today. Full details of the simulations may be found in Bush and Philander (1999) and Bush (1999). A general model overview is provided in another paper in this volume (Bush, 2002-this volume). However, two numerical schemes of relevance to the present study are the soil moisture scheme and the surface albedo scheme, so they will be outlined here.

Soil moisture in the model is predicted according to a simple bucket scheme that uses a field capacity of 15 cm. Evaporation from soils that have 11.25 cm or greater water content is equal to evaporation from a saturated surface. Evaporation from drier surfaces is reduced from that of a saturated surface by the ratio of

the actual soil moisture to the field capacity. Water in excess of 15 cm is re-routed as river runoff.

The albedo of bare land surfaces is initially prescribed but may be modified during the integration by snowfall. There is thus no interactive vegetation in this model. Although vegetation–climate feedbacks are known to be important in contributing to the location of desert margins in the sub-Sahel (e.g., Kutzbach et al., 1996, 1998; Zeng et al., 1999), we are in the present study restricted to examining the large-scale atmospheric changes that trigger such feedbacks. In the LGM simulation, surface albedos were taken from a dataset compiled by CLIMAP (1981) so that, in some sense, they already account for estimated LGM vegetation in the area of interest. For simplicity, albedos for the mid-Holocene simulation are taken to be the same as today (although it is known that there were changes in biomes; e.g., Williams et al., 2000).

Vertical discretization in the model is done in terms of σ coordinates, where σ, a normalized pressure coordinate, is defined by $\sigma = P/P^*$ (P^* is equal to surface pressure). Model levels are unevenly spaced at σ=0.015, 0.05, 0.101, 0.171, 0.257, 0.355, 0.46, 0.568, 0.676, 0.777, 0.866, 0.935, 0.979, and 0.997. These coordinates are used, rather than pressure surfaces, because they are a terrain-following coordinate and are, hence, not intersected by model topography. In Section 4, figures show planform plots of winds on σ-surfaces. Analysis on σ levels makes it easier to interpret circulation anomalies at high elevations, such as over the Loess Plateau, and relate them to lower tropospheric anomalies on the same σ level.

3. Results from the Loess Plateau

Grain size analyses of loess–paleosol sequences have been used as proxies for paleoclimatic conditions by many workers (e.g., Rutter, 1992; Ding et al., 1993, 1994). The ratio of the fraction of particles less than 2 μm (wt.%) to the fraction of particles greater than 10 μm (wt.%) is termed the grain size index. This index is very sensitive to loess–soil alternations (Ding et al., 1994) and is therefore a good indicator of deposition paleoenvironments. Geochronological control of the sequences is based on magnetostratigraphy (Rutter et al., 1991) combined with an orbital time scale (Ding et al., 1994), as well as ^{14}C and thermoluminescence dating (Sun et al., 1998b).

Grain size analysis from four sites along the Plateau (Yulin, Fang Ta, Dayancha, and Wupu) clearly reveals the glacial–interglacial transition from coarse to fine grain size deposits, respectively (Fig. 1). The analysis also indicates that, in general, there is more deposition during glacial periods than during interglacials. There is also a gradual thinning of deposits from northwest to southeast as distance from the particle source increases.

Based on grain size analysis of the loess sequences, the locations of the desert margin at the LGM and in the mid-Holocene, relative to today, have been estimated (Fig. 2). Note that the margin locations are not exact and will most likely change as new data are collected (even for the present margin). Nevertheless, the migration pattern shown is such that the desert margin at the LGM was farther southeast than today, indicating drier conditions and desert expansion, whereas it was farther northwest during the mid-Holocene, indicating moister conditions and desert retreat. Because of the lack of data, the exact location of the mid-Holocene margin is not known (as noted by the arrow in Fig. 2).

4. Model results: mid-Holocene

In the mid-Holocene simulation, annual mean winds near the surface over northern China were primarily from the north/northwest, as they are today (Fig. 3). This implies that deposition on the Loess Plateau (near 37°N, 110°E) at this time would still have been regulated by the climatological northerly/northwesterly winds, as has been suggested for times throughout the last glacial cycle (Lu and Sun, 2000).

However, the wind difference indicates that the westerly wind component over this region was weaker because of a cyclonic circulation over the Tibetan Plateau (Fig. 3c). This circulation anomaly was the result of increased latent heat release by an enhanced south Asian monsoon during the summer months of June–July–August (JJA; see Bush, 2002-this volume). This circulation anomaly increased surface convergence over the western portion of the Loess Plateau, and precipitation averaged from 100°E–115°E and 32°N–40°N increased by 13%. Despite the fact that the area was nearly 2 °C warmer during the mid-

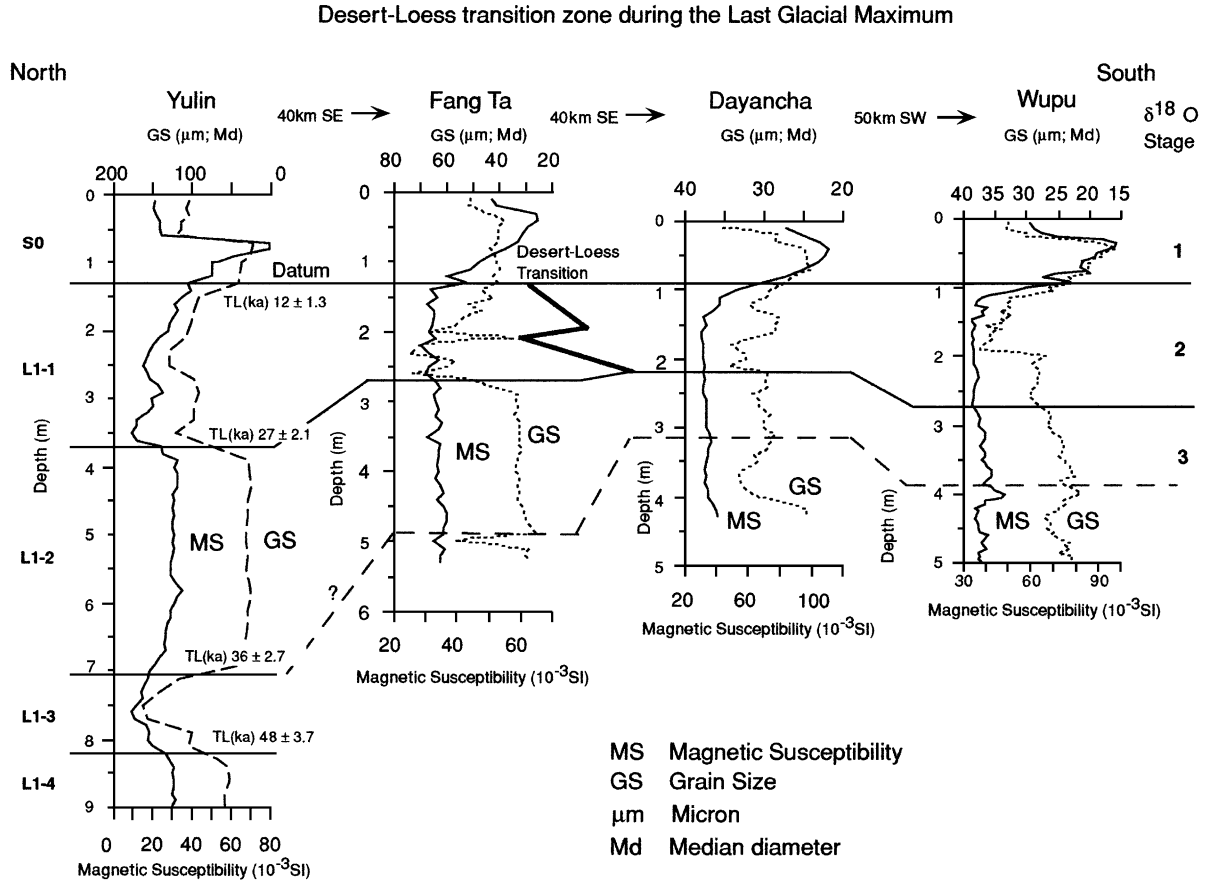

Fig. 1. Cross-section along the desert-loess transition zone during the last glacial period. Thermoluminsescence chronology is from Sun et al. (1995, 1998b). Samples were taken every 10 cm. Grain size analysis was performed on a PRO-700 SK Laser Micron Sizer. An analysis of 20 replicate samples indicated a precision of ±3.5%. Bulk magnetic susceptibility was determined using a Bartington MS-2 susceptibility meter. Magnetic susceptibility values represent one reading on an approximately 50-g bagged sample.

Holocene summertime, evaporation increased by only 4% because of weaker wind speeds.

Mean annual freshwater flux was therefore increased over the Plateau region, and there was a general wetting of the land surface (Fig. 4). North of 45°N, however, there was increased subsidence and a drying of the surface. This subsidence was caused by large-scale descent of the northern branch of the cyclonic winds, and was an amplification of the descent that occurs today during the summer monsoon months (see Broccoli and Manabe, 1997).

For our purposes, the desert margin in the simulations is defined as the 2-cm soil moisture content contour which, in the control simulation, bounds the Taklimakan Desert to the west and a majority of the Gobi Desert to the east (bold line in Fig. 4a). Soil moisture is a reasonable indicator of aridity because its numerical calculation involves all the variables that are involved in the more classic definitions of climate zones such as the Köppen classification (e.g., Lamb, 1972). In particular, regions of low soil moisture have been shown to correlate well with Köppen category B climates (desert and steppe; Broccoli and Manabe, 1997) and so will be used as an indicator of surface aridity in these simulations.

Model results indicate that, although there was not much change in the northern desert boundary near 45°N, there was a northwestward migration of the southeastern boundary (Fig. 4b). As this boundary migration is below the equivalent resolution of the

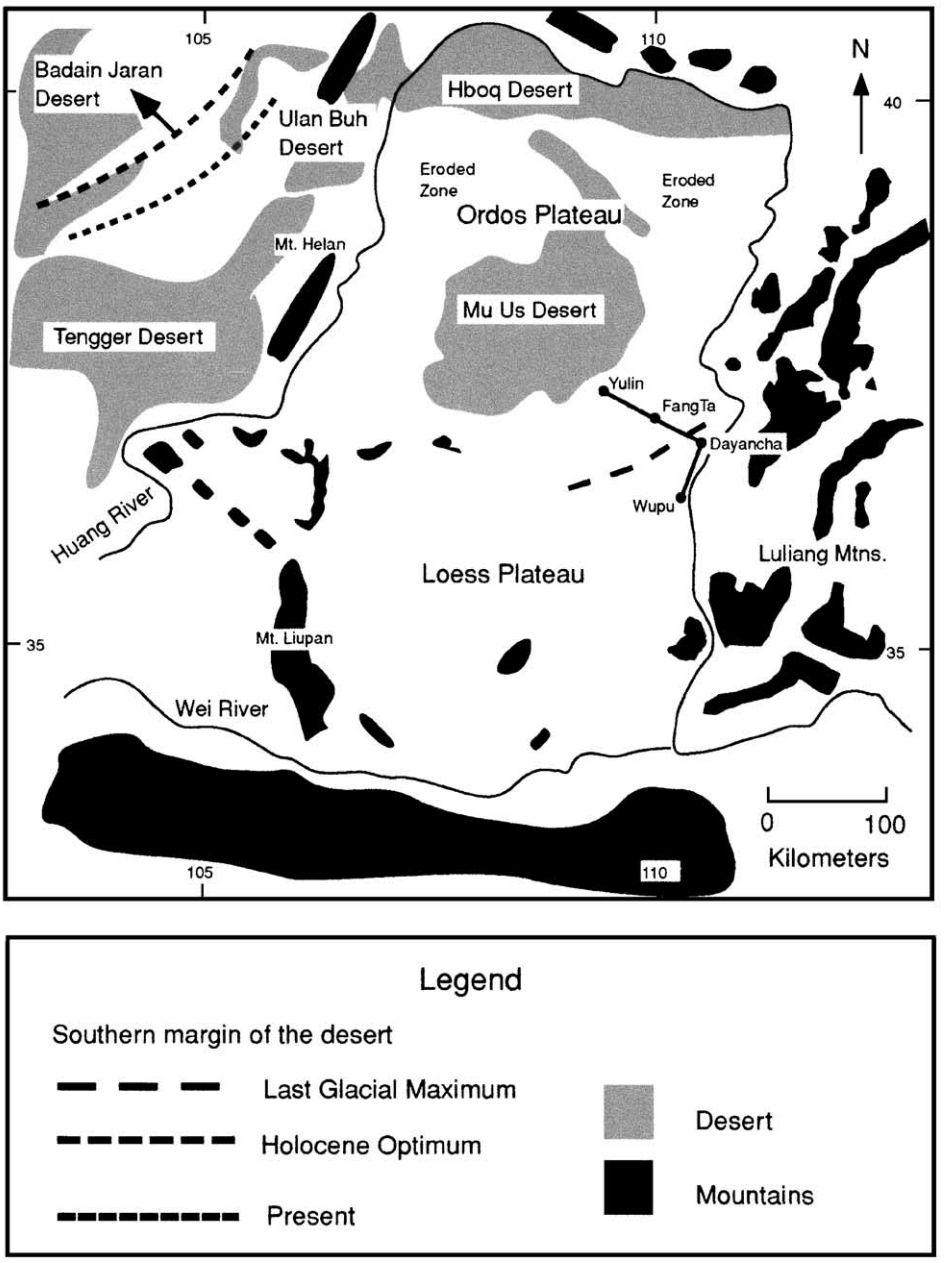

Fig. 2. Map of the southern margin of the Chinese deserts during the Last Glacial Maximum, the mid-Holocene, and the present day. The modern desert margin coincides with the 100-mm mean annual precipitation isohyet (Zhao, 1986). The desert margins were modified from Sun and Ding (1998). The location of the uplands was modified using Operational Navigation Charts Sheets F-7, F-8, G-8, G-9 from the U.S. Department of Defense (1987).

model, we determine the statistical significance of wetting in the region by a simple *t*-test for soil moisture averaged over the region 95°E–110°E and 37°N–42°N (which encompasses the southeastern desert margin). Averaged in time, soil moisture in this area is 2.079 in the control simulation with a variance

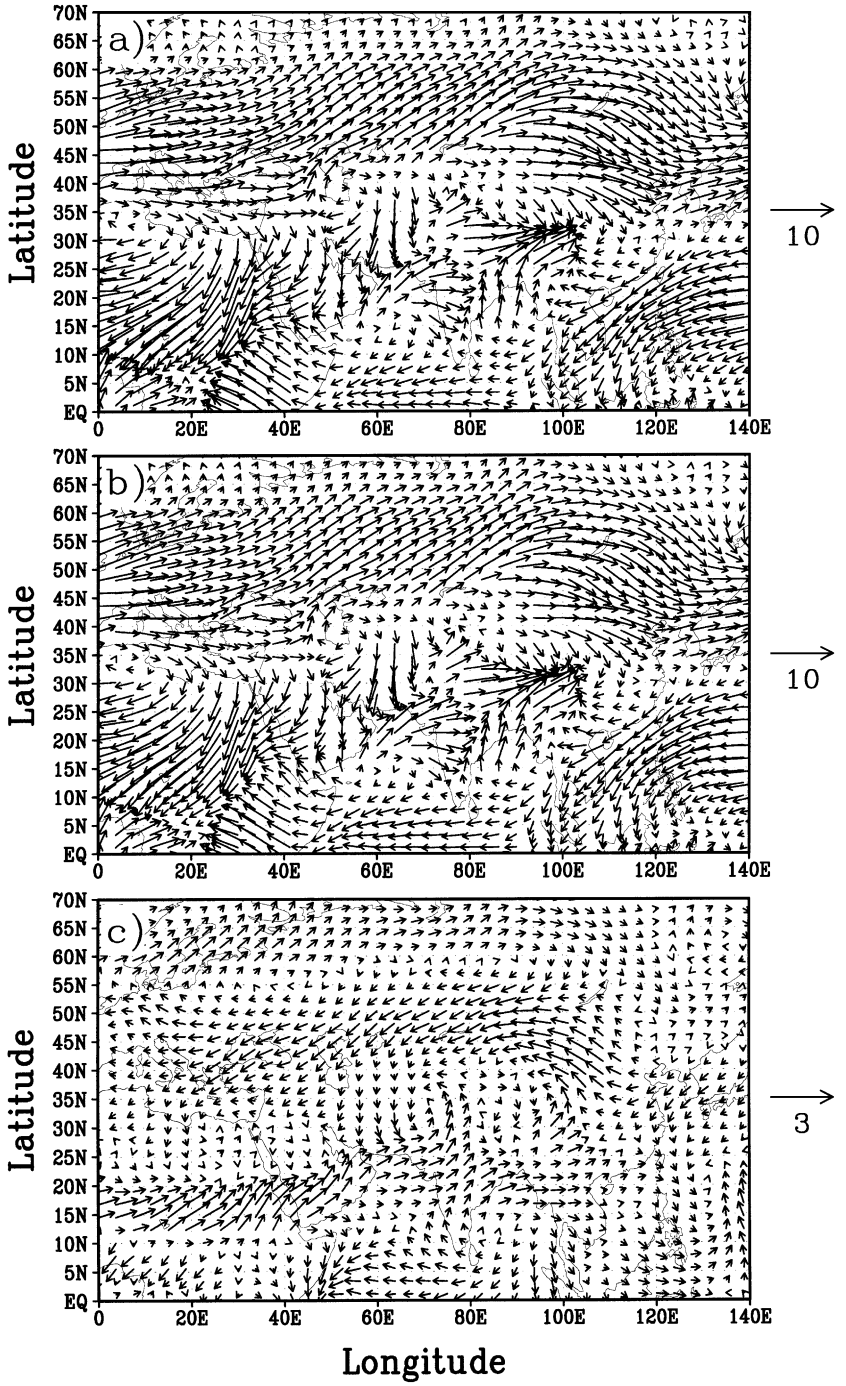

Fig. 3. Annual mean winds on the second model level (σ=0.979) in (a) the control simulation and (b) the mid-Holocene simulation. Differences in these winds (experiment minus control) are shown in (c). See Section 2 for a description of the model levels. Units are m/s as indicated. Note that the wind vectors in (c) are scaled differently.

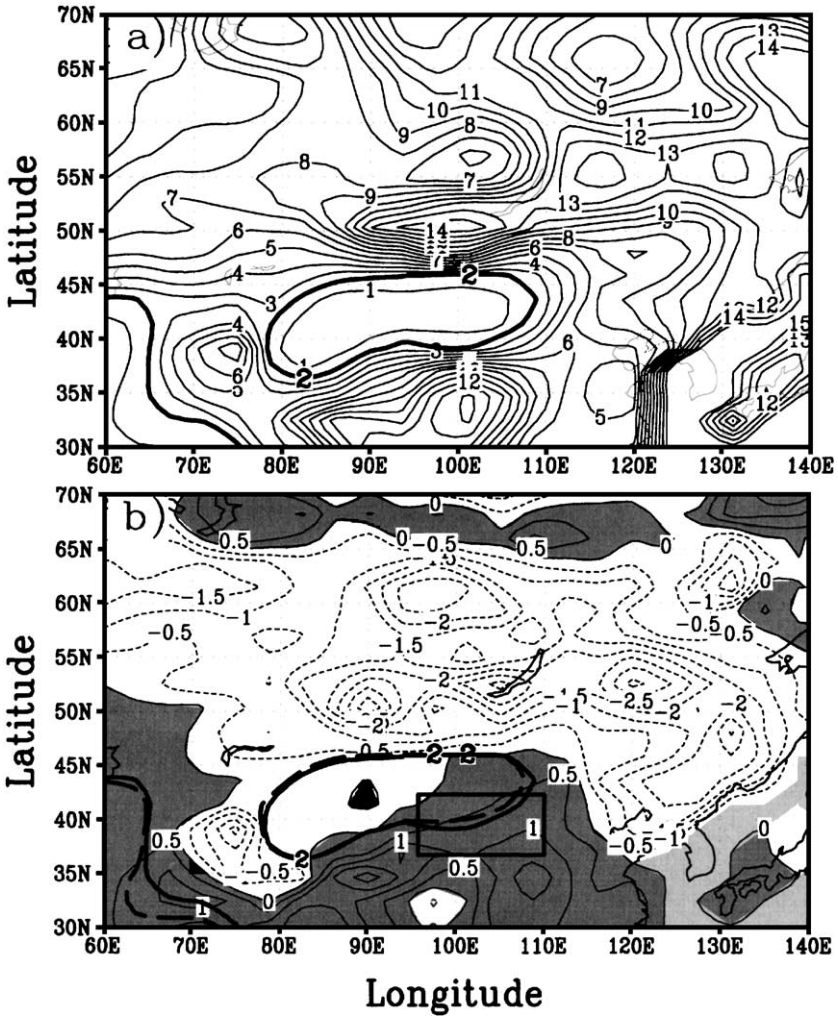

Fig. 4. (a) Annual mean soil moisture amount in the control simulation. (b) The soil moisture difference (experiment minus control). Units are cm water. The contour interval is 1 cm in (a) and 0.5 cm in (b). Dark shading in (b) indicates regions that are wetter than today. The rectangle indicates the region that includes the field sites and in which the statistical analysis is done.

of 0.0086 (191 degrees of freedom). In the mid-Holocene simulation, the mean is 2.756 with a variance of 0.0158 (191 degrees of freedom). Moistening of this region is therefore statistically significant at more than the 99% confidence level.

Simulated migration of the desert margin is in the same geographical direction as that inferred from loess sequences, although it is most likely underestimated in the model since vegetation feedbacks are ignored and spatial resolution is relatively coarse for this type of comparison. Nevertheless, temporal stability of area-averaged soil moistures indicates that the climatic conditions responsible for the simulated change were driven by persistent, large-scale atmospheric conditions and, in particular, by changes in the mean summer monsoon as described above.

5. Model results: Last Glacial Maximum

Annual mean winds near the surface in the LGM simulation indicate that, as in the mid-Holocene

simulation, winds over the Loess Plateau were primarily from the north/northwest (Fig. 5a). The wind difference (Fig. 5b) indicates that the westerly component in this region was stronger, however, this was because of changes in the westerly monsoon winds during the summer months of JJA (see Bush, this volume).

The westerly midlatitude jet at 50–55°N is weaker in the LGM simulation because of anticyclonic flow around the cold, high pressure zone over the Fennoscandian ice sheet (centered near 25°E, 60°N). This anomalous circulation is extensive and weakens winds over central Asia throughout the entire troposphere (Fig. 6). North/northwest of the Tibetan Plateau, modeling shows an anomalous upper level convergence between the westerly trades, which exhibit not only reduced speeds but more anticyclonic curvature downstream of the ice sheet and an upper level anticyclone over the Plateau (marked by an "H" in Fig. 6b). This anticyclone is caused in part by low-level convergence and ascent during the summer months, as well as by northerly flow towards a site of strong upper level divergence over the exposed Sunda shelf.

In addition to forming strong upper tropospheric convergence over the Loess Plateau region, the ice sheet also induced large-scale subsidence over the region west and north of the Tibetan Plateau (Fig. 7). Averaged from 40°E to 90°E and from 30°N to 70°N,

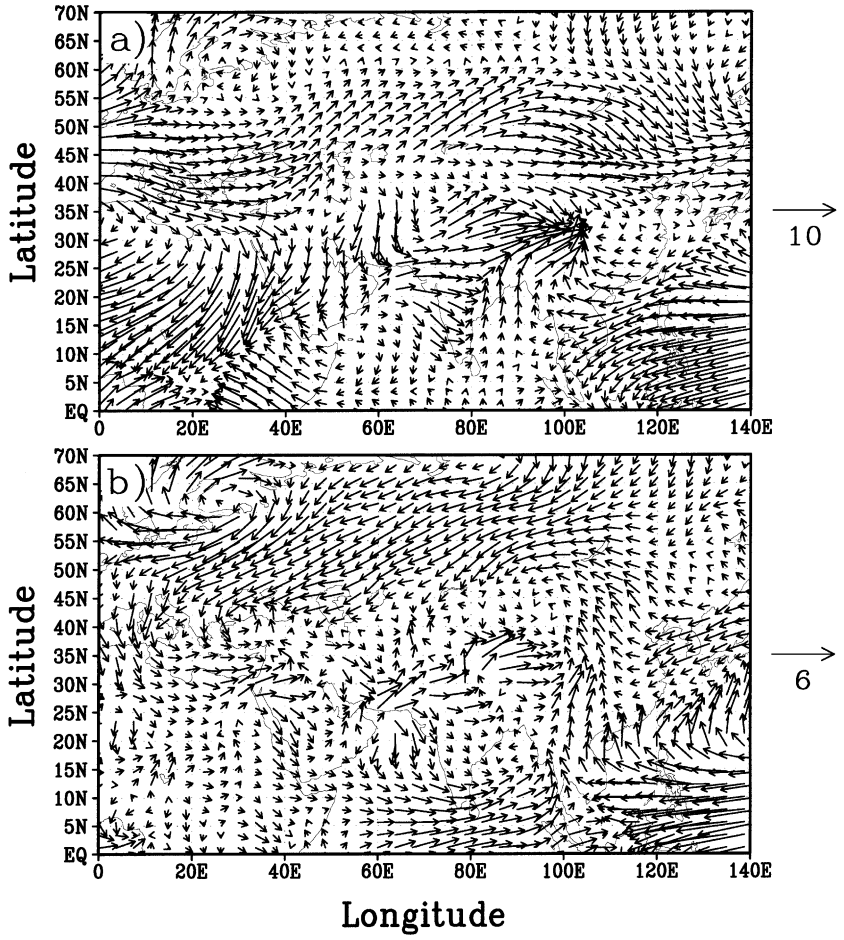

Fig. 5. (a) Annual mean winds on the second model level (σ=0.979) in the LGM simulation (see text for a description of the model levels). Differences (LGM minus control) are shown in (b). Units are m/s as indicated. Note that the wind vectors in (b) are scaled differently.

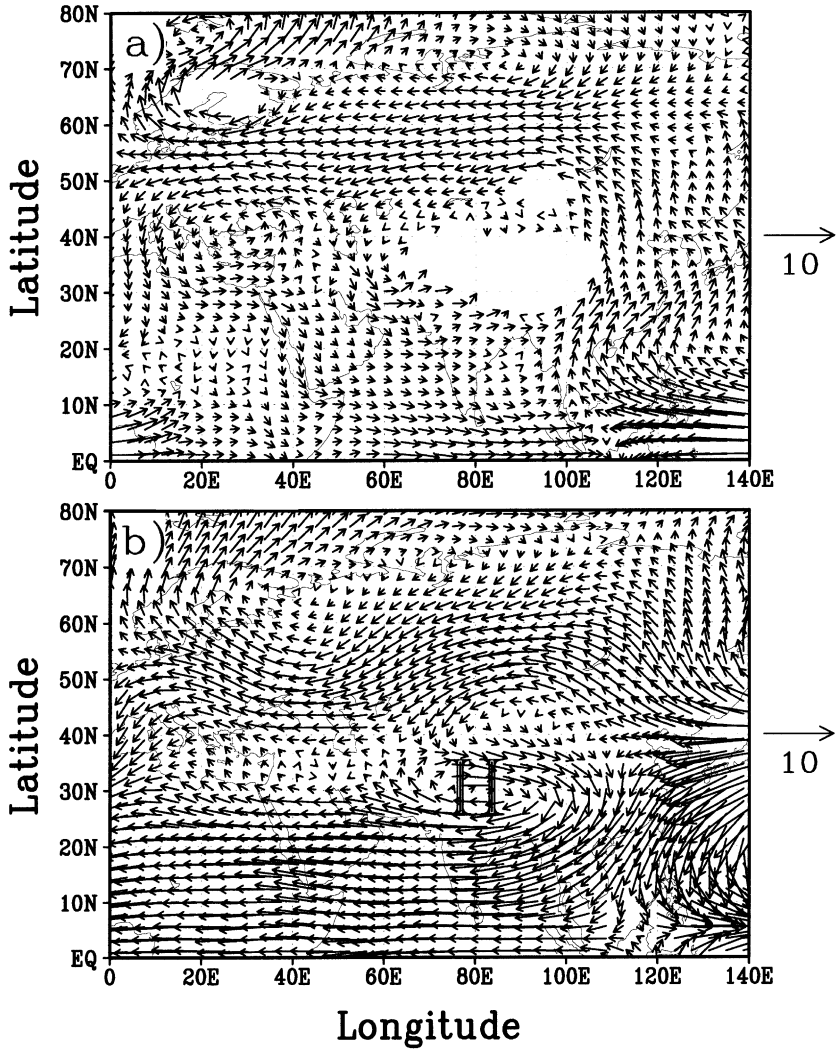

Fig. 6. Difference (LGM minus control) in the annual mean winds in (a) the lower troposphere (850 mb) and (b) the upper troposphere (250 mb). Units are m/s as indicated. No vectors are plotted where the pressure surface lies below the Earth's surface.

there was a 19% increase in mid-tropospheric subsidence. This subsidence suppresses precipitation and decreases soil moisture across much of north-central Asia. Anomalous upper level wind convergence was strongest, however, in the region above the Plateau (cf. Fig. 6b).

Averaged over the region 95°E–110°E and 37°N–42°N, annual mean soil moisture was 1.958 with a variance of 0.0161 (59 degrees of freedom), so there was a net drying of approximately 6% compared to today. This drying is statistically significant at the 88% confidence level. However, there is not much simulated change in the eastern desert boundary near the Loess Plateau (Fig. 8). The western margin, on the other hand, expanded to the west and northwest to the Kara Kum (east of the Caspian Sea) as a result of the increased large-scale subsidence over the region. Although the simulated soil moisture changes do not produce a significant southeastward migration of the desert margin, simulated drying near the Loess Plateau does agree with inferences made from loess–paleosol sequences.

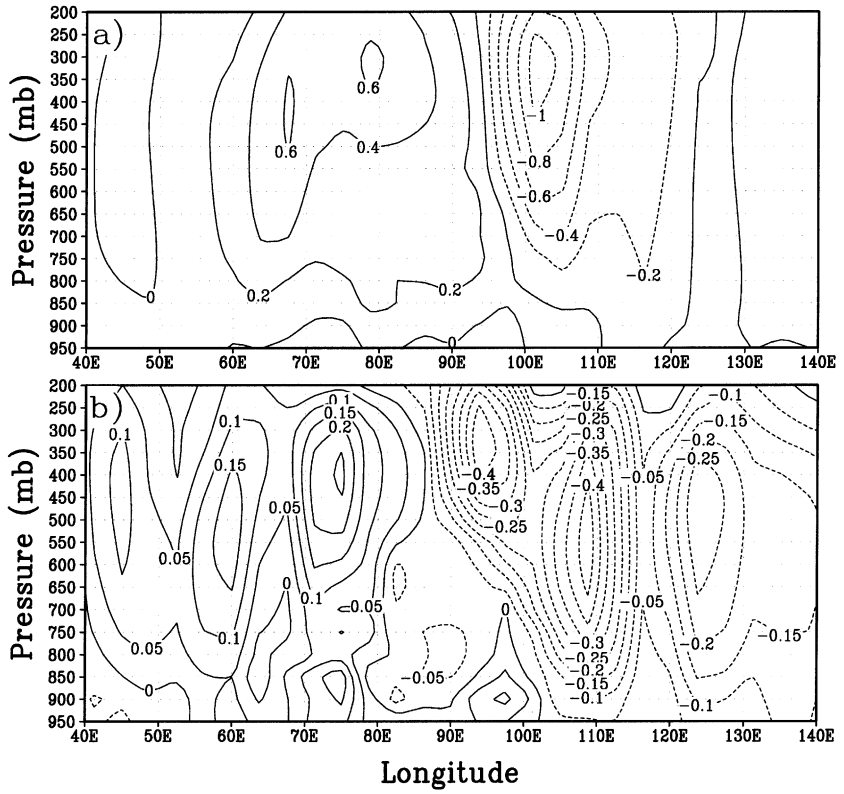

Fig. 7. (a) Longitude–height cross-section of the annual mean vertical pressure velocity averaged between the latitudes of 25°N and 60°N. Positive values indicate downward motion, and negative values indicate rising motion. Units are dyn cm^{-2} s^{-1}.

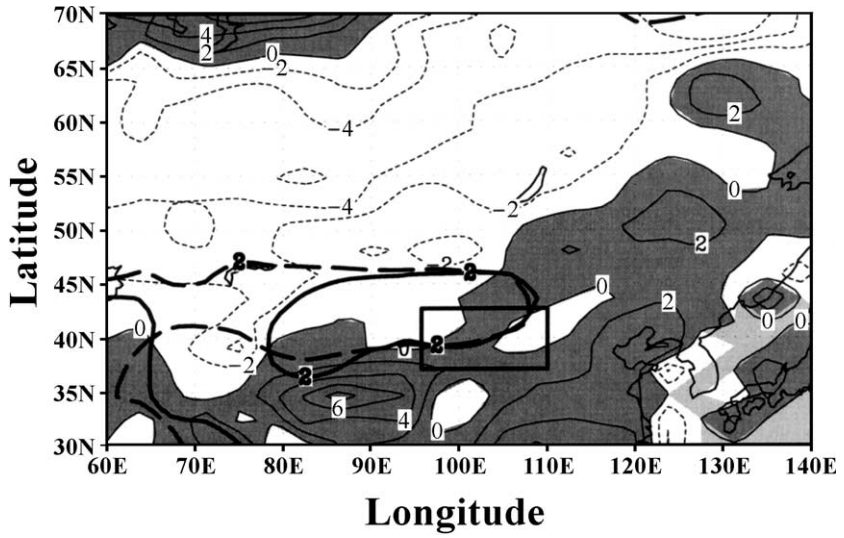

Fig. 8. Difference in annual mean soil moisture (LGM minus control). Units are cm water. The contour interval is 1 cm in (a) and 0.5 cm in (b). Dark shading in (b) indicates regions that are wetter than today. The rectangle indicates the region that includes the field sites and in which the statistical analysis is done.

6. Discussion

Migration of climatic zones through the late Quaternary has dramatically influenced land surface processes and the biomes that they support (e.g., Webb et al., 1998; Prentice et al., 1991; Wright et al., 1993). For arid regions, such as central Asia, loess can be used to distinguish between dry, glacial climates and wetter, interglacial climates. The Chinese Loess Plateau, in particular, appears to have been in close proximity to a desert throughout the Quaternary given its continuous record of loess deposits (e.g., Rutter et al., 1996).

The task of determining where the desert margin was at the time in question, however, is exceedingly complex because it depends on such factors as precipitation, evaporation, and radiation, as well as wind direction and strength. One method of estimating how these quantities were different in the past is to perform direct numerical simulations. We have therefore analysed the factors that play a role in changing the surface hydrology (as a proxy for desert conditions) in a set of GCM experiments. Comparison of field data with GCM results is complicated by the difference in spatial scales, so the model data are analysed for significance and for the large-scale dynamics from which surface hydrology is calculated.

The mid-Holocene simulation exhibits a statistically significant wetting of the soil surface in the region of the Loess Plateau. Migration of the soil moisture contour used to denote the desert margin was from southeast to northwest, in agreement with the direction of migration inferred from the loess record based on grain size analysis (Sun et al., 1999). The enhanced summer monsoon circulation is consistent with other modelling studies of the mid-Holocene (e.g., Kutzbach and Otto-Bliesner, 1982; Prell and Kutzbach, 1992) and is shown here to have been responsible for the hydrological changes north of the Tibetan Plateau. In particular, the stronger cyclonic cell over the Tibetan Plateau converges winds and increases precipitation over the western part of the Loess Plateau near 105°E.

Nevertheless, simulated aridity exhibits spatial variability, with some regions becoming wetter and some becoming drier (cf. Fig. 4). This variability is linked in part to the patterns of large-scale uplift and subsidence. The vertical circulation associated with the modern summer monsoon is characterized by low-level convergence, precipitation, and latent heat release over the Tibetan Plateau. A low-level cyclonic cell is thus formed in this region of uplift and divergence and an anticyclonic circulation forms in the upper troposphere. Upper level convergence, subsidence, and surface aridity then occurs north and west of the Tibetan Plateau (Broccoli and Manabe, 1997). The strength of these circulations depends upon the strength of the low-level monsoon and the latent heat that is released. In the mid-Holocene, this monsoon circulation was strengthened by the radiative changes induced by the Earth's orbital parameters, and increased precipitation over the Loess Plateau and increased drying further north are consequences.

It is the summer monsoon, therefore, that determines the strength of the cyclonic low, and it is the interaction of this low with the trade westerlies that governs the mean moisture flux and winds over the Loess Plateau region. Since these are the primary factors that determine soil moisture and, hence, by inference, loess texture, this analysis suggests that it is the strength of the summer monsoon, rather than that of the winter monsoon, that is a critical factor in determining desert margins near the Plateau.

In the LGM simulation, soil moisture also exhibits a high degree of spatial variability, although the changes (in particular, the drying in central Asia) have a greater magnitude than in the mid-Holocene simulation. Although there is an overall drying of 6% over the Loess Plateau region, the simulated southeast desert margin, as represented by soil moisture, remains in approximately the same position. There is, however, a large expansion of the northern desert margin toward the northwest and west (cf. Fig. 8) in agreement with palynological, pedological, and sedimentological evidence (Lioubimtseva et al., 1998). One component of the LGM drying may be attributed to the almost 10% decrease in the hydrological cycle (which is coupled to decreased atmospheric CO_2; Bush and Philander, 1999), although the large increase in tropospheric subsidence downstream of the Fennoscandian ice sheet is responsible for drying over much of central-western Asia.

It is known, however, that particle deposition in the region of the Loess Plateau is not governed by the relatively slow, climatological winds but rather by episodic and comparatively violent haboob-type fron-

tal flows that are turbulent enough to suspend and transport particles vast distances from the source region (e.g., Deer, 1984; Pye, 1987; Middleton, 1991; Mitsuta et al., 1995; Simpson, 1997). Associating the strata of relatively coarse-grained deposits in a sequence with dry glacial conditions and the proximity of an expanded desert, while associating the strata of finer-grained deposits with moist interglacial periods and a shrunken desert, is to over-simplify the mechanisms by which these deposits came into being. Haboob-type flows are also known as gravity currents, and their structure can be divided into three distinct parts: the head, the body, and the tail. The head of a gravity current has a distinct shape: it is generally thicker than the body or tail by a factor of approximately two, and it exhibits stronger turbulent suspension than either the body or the tail. The head is therefore able to carry much coarser sediment than the body of the current, and it can keep them suspended for a longer time than the body can suspend finer particles. It is therefore possible for some coarse grains to bypass more proximal regions where fine grains would be deposited from the body and tail of the current. Some coarse particles, therefore, may not be deposited adjacent to the source, but farther downstream.

In addition, recent aqueous experiments (Gladstone et al., 1998) have shown that there is another mechanism by which the distance that coarse particles are transported may be substantially increased. Adding small amounts of fine sediment to a coarse-grained particle suspension in a gravity current has a much larger influence on flow velocity, run-out distance, and sedimentation pattern than adding a small amount of coarse sediment to a fine-grained gravity current. The experiments show that adding small amounts of fine particles to a coarse-grained particle suspension current in water results in enhanced flow velocities and enhanced transport of coarse particles. The particle mixtures created in the laboratory currents could be analogous to those present in the air currents that produced the loess sequences, and this suggests that the grain-size distribution of the desert source is another important factor in determining the geographical pattern of deposition.

While simulation of haboob-type flows is beyond the capability of modern GCMs, the synoptic conditions out of which they emerge (and which has been shown here to be different than today at both time periods) is likely to have altered the spatial distribution of deposits throughout the Quaternary. Further work on sections from the Loess Plateau is in progress in an attempt to link spatial patterns of grain-size and deposition amounts to the known deposition pattern of gravity currents and haboob-type flows that are spawned by the synoptic-scale flow.

7. Conclusions

We have demonstrated that numerical simulations for the mid-Holocene and for the LGM give statistically significant wetting and drying of the Loess Plateau region, respectively. Moreover, these trends and the migration of the desert margin that they imply are similar to those suggested by grain size analysis of loess–paleosol sequences taken from the Chinese Loess Plateau. Analysis of the model results indicates that it was the increased intensity of the summer monsoon that was responsible for the mid-Holocene wetting. Drying at the LGM was a combination of a reduced hydrological cycle as well as an increase in large-scale subsidence over western Asia in response to orographic downstream effects of the Fennoscandian ice sheet. While the model neglects important factors such as vegetation–climate feedbacks as well as mesoscale air currents, it nevertheless reproduces the first-order changes in surface hydrology that have been inferred from sequence stratigraphy.

References

Broccoli, A.J., Manabe, S., 1997. Mountains and midlatitude aridity. In: Ruddiman, W.F. (Ed.), Tectonic Uplift and Climate Change. Plenum, New York, pp. 89–121.

Bush, A.B.G., 1999. Assessing the impact of mid-Holocene insolation on the atmosphere–ocean system. Geophys. Res. Lett. 26, 99–102.

Bush, A.B.G., 2002. A comparison of simulated monsoon circulations and snow accumulation in Asia during the mid-Holocene and at the Last Glacial Maximum. Global Planet. Change 33.

Bush, A.B.G., Philander, S.G.H., 1999. The climate of the Last Glacial Maximum: results from a coupled atmosphere–ocean general circulation model. J. Geophys. Res. 104, 24509–24525.

Climate: Long-Range Investigation, Mapping, and Prediction (CLIMAP) Project Members, 1981. Seasonal reconstructions of the Earth's surface at the last glacial maximum. Map and Chart Series MC-36. Geol. Soc. Am., Boulder, CO.

Deer, Z., 1984. Synoptic-climatic studies of dust fall in China since historic times. Sci. Sin. 27, 825–836.

Ding, Z.L., Rutter, N.W., Liu, T., 1993. Pedostratigraphy of Chinese loess deposits and climatic cycles in the last 2.5 Ma. Catena 20, 73–91.

Ding, Z.L., Yu, Z., Rutter, N.W., Liu, T., 1994. Towards an orbital time scale for Chinese loess deposits. Quat. Sci. Rev. 13, 39–70.

Ding, Z.L., Sun, J.M., Rutter, N.W., Rokosh, D., Liu, T.S., 1999. Changes in sand content of loess deposits along a north–south transect of the Chinese Loess Plateau and the implications for desert variations. Quat. Res. 52, 56–62.

Gladstone, C., Phillips, J.C., Sparks, R.S.J., 1998. Experiments on bidisperse, constant-volume gravity currents: propagation and sediment deposition. Sedimentology 45, 833–843.

Guo, Z.T., Liu, T.S., Fedoroff, N., Wei, L.Y., Ding, Z.L., Wu, N.Q., Lu, H.Y., Jian, W.Y., An, Z.S., 1998. Climate extremes in Loess of China coupled with the strength of deep-water formation in the North Atlantic. Global Planet. Change 18, 113–128.

Hall, N.M.J., Valdes, P.J., Dong, B., 1996. The maintenance of the last great ice sheets: A UGAMP GCM study. J. Clim. 9, 1004–1019.

Kutzbach, J.E., Otto-Bliesner, B.L., 1982. The sensitivity of the African–Asian monsoonal climate to orbital parameter changes for 9000 years B.P. in a low-resolution general circulation model. J. Atmos. Sci. 39, 1177–1188.

Kutzbach, J.E., Wright, H.E., 1985. Simulation of the climate of 18,000 yr BP: results for the North American/North Atlantic/European sector and comparison with the geologic record. Quat. Sci. Rev. 4, 147–187.

Kutzbach, J.E., Bonan, G., Foley, J., Harrison, S.P., 1996. Vegetation and soil feedbacks on the response of the African monsoon to orbital forcing in the early to middle Holocene. Nature 384, 623–626.

Kutzbach, J.E., Gallimore, R., Harrison, S., Behling, P., Selin, R., Laarif, F., 1998. Climate and biome simulations for the past 21,000 years. Quat. Sci. Rev. 17, 473–506.

Lamb, H.H., 1972. Climate: Present, Past and Future. Methuen, London.

Lioubimtseva, E., Simon, B., Faure, H., Faure-Denard, L., Adams, J.M., 1998. Impacts of climatic change on carbon storage in the Sahara–Gobi desert belt since the last glacial maximum. Global Planet. Change 17, 95–105.

Lu, H.Y., Sun, D.H., 2000. Pathways of dust input to the Chinese Loess Plateau during the last glacial and interglacial periods. Catena 40, 251–261.

Lu, H.Y., VanHuissteden, K.O., An, Z.S., Nugteren, G., Vandenberghe, J., 1999. East Asia winter monsoon variations on a millennial time-scale before the last glacial–interglacial cycle. J. Quat. Sci. 14, 101–110.

Lu, H.Y., VanHuissteden, K.O., Zhou, J., Vandenberghe, J., Liu, X.D., An, Z.S., 2000. Variability of East Asian winter monsoon in Quaternary climatic extremes in North China. Quat. Res. 54, 321–327.

Mahowald, N., Kohfeld, K., Hansson, M., Balkanski, Y., Harrison, S.P., Prentice, I.C., Schulz, M., Rodhe, H., 1999. Dust sources and deposition during the last glacial maximum and current climate: a comparison of model results with paleodata from ice cores and marine sediments. J. Geophys. Res. 104, 15895–15916.

Manabe, S., Broccoli, A.J., 1985. The influence of continental ice sheets on the climate of an Ice Age. J. Geophys. Res. 90, 2167–2190.

Middleton, N.J., 1991. Dust storms in the Mongolian People's Republic. J. Arid Environ. 20, 287–297.

Mitsuta, Y., Hayashi, T., Takemi, T., 1995. Two severe local storms as observed in the arid area of northwest China. J. Meteorol. Soc. Jpn. 73, 1269–1284.

Molina-Cruz, A., 1977. The relation of the southern trade winds to upwelling processes during the last 75,000 years. Quat. Res. 8, 324–338.

Pedersen, T.F., 1983. Increased productivity in the eastern equatorial Pacific during the last glacial maximum (19,000 to 14,000 yr B.P.). Geology 11, 16–19.

Petit, J.R., Briat, M., Royer, A., 1981. Ice age aerosol content from East Antarctic ice core samples and past wind strength. Nature 293, 391–394.

Petit, J.R., et al., 1990. Palaeoclimatological and chronological implications of the Vostok core dust record. Nature 343, 56–58.

Porter, S.C., An, Z.S., 1995. Correlation between climate events in the North Atlantic and China during last glaciation. Nature 375, 305–308.

Prell, W.L., Kutzbach, J.E., 1992. Sensitivity of the Indian monsoon to forcing parameters and implications for its evolution. Nature 360, 647–652.

Prentice, I.C., Bartlein, P.J., Webb III, T., 1991. Vegetation and climate changes in eastern North America since the last glacial maximum: a response to continuous climatic forcing. Ecology 72, 2038–2056.

Pye, K., 1987. Aeolian Dust and Dust Deposits. Academic Press, New York, 334 pp.

Rack, F.R., Rutter, N.W., Bush, A.B.G., Rokosh, D., Ding, Z., 2000. Linking palaeoclimate ocean and continental (loess) records. Can. J. Earth Sci., 37, 831–848.

Rutter, N.W., 1992. Presidential Address, XIII INQUA Congress 1991: Chinese loess and global change. Quat. Sci. Rev. 11, 275–281.

Rutter, N.W., Ding, Z.L., Evans, M.E., Wang, Y., 1991. Magnetostratigraphy of the Baoji loess–paleosol section in the north-central China Loess Plateau. Quat. Int. 7/8, 97–192.

Rutter, N.W., Ding, Z., Liu, T., 1996. Long paleoclimate records from China. Geophysica 32, 7–34.

Sarnthein, M., Tetzlaff, G., Koopman, B., Wolter, K., Pflaumann, U., 1981. Glacial and interglacial wind regimes over the eastern subtropical Atlantic and north-west Africa. Nature 293, 193–196.

Simpson, J.E., 1997. Gravity Currents in the Environment and the Laboratory, 2nd edn. Cambridge Univ. Press, Cambridge, UK, 244 pp.

Sun, J.M., Ding, Z.L., 1998. Deposits and soils of the past 130,000 years at the desert-loess transition in Northern China. Quat. Res. 50, 148–156.

Sun, J.M., Ding, Z.L., Liu, T.S., 1995. The environmental evolution of the desert-loess transitional zone over the last glacial–interglacial cycle. Scientia Geologica Sinica. Science Press, Beijing, China, 1–8.

Sun, J.M., Ding, Z.L., Liu, T.S., 1998a. Desert distribution during the glacial maximum and climatic optimum: example of China. Episodes 21, 28–30.

Sun, J.M., Ding, Z.L., Liu, T.S., Chen, J., 1998b. Thermoluminescence chronology of sand profiles in the Mu Us Desert, China. Palaeogeogr., Palaeoclimatol., Palaeoecol. 144, 225–233.

Sun, J.M., Ding, Z.L., Liu, T.S., Rokosh, D., Rutter, N.W., 1999. 580,000-year environmental reconstruction from aeolian deposits at the Mu Us desert margin, China. Quat. Sci. Rev. 18, 1351–1364.

Texier, D., de Noblet, N., Braconnot, P., 2000. Sensitivity of the African and Asian monsoons to mid-Holocene insolation and data-inferred surface changes. J. Clim. 13, 164–181.

U.S. Defence Mapping Agency Aerospace Center, 1987. Operational Navigation Chart Series ONC, Sheets F-7, F-8, G-8, G-9, Scale 1:1,000,000.

Vandenberghe, J., An, Z.S., Nugteren, G., Lu, H.Y., VanHuissteden, K., 1997. New absolute time scale for the Quaternary climate in the Chinese loess region by grain-size analysis. Geology 25, 35–38.

Webb III, T., Anderson, K.H., Bartlein, P.J., Webb, R.S., 1998. Late Quaternary climate change in eastern North America: a comparison of pollen-derived estimates with climate model results. Quat. Sci. Rev. 17, 587–606.

Williams, J.W., Webb III, T., Richard, P.H., Newby, P., 2000. Late Quaternary biomes of Canada and the eastern United States. J. Biogeogr. 27, 585–607.

Wright Jr., H.E., Kutzbach, J.E., Webb III, T., Ruddiman, W.F., Street-Perrott, F.A., Bartlein, P.J. (Eds.), 1993. Global Climates Since the Last Glacial Maximum. University of Minnesota Press, Minneapolis, 569 pp.

Zeng, N., Neelin, J.D., Lau, K.M., Tucker, C.J., 1999. Enhancement of interdecadal climate variability in the Sahel by vegetation interaction. Science 286, 1537–1540.

Zhao, S., 1986. Physical Geography of China. Science Press, Beijing, 209 pp.